biomolecules

IMPACT FACTOR 4.694

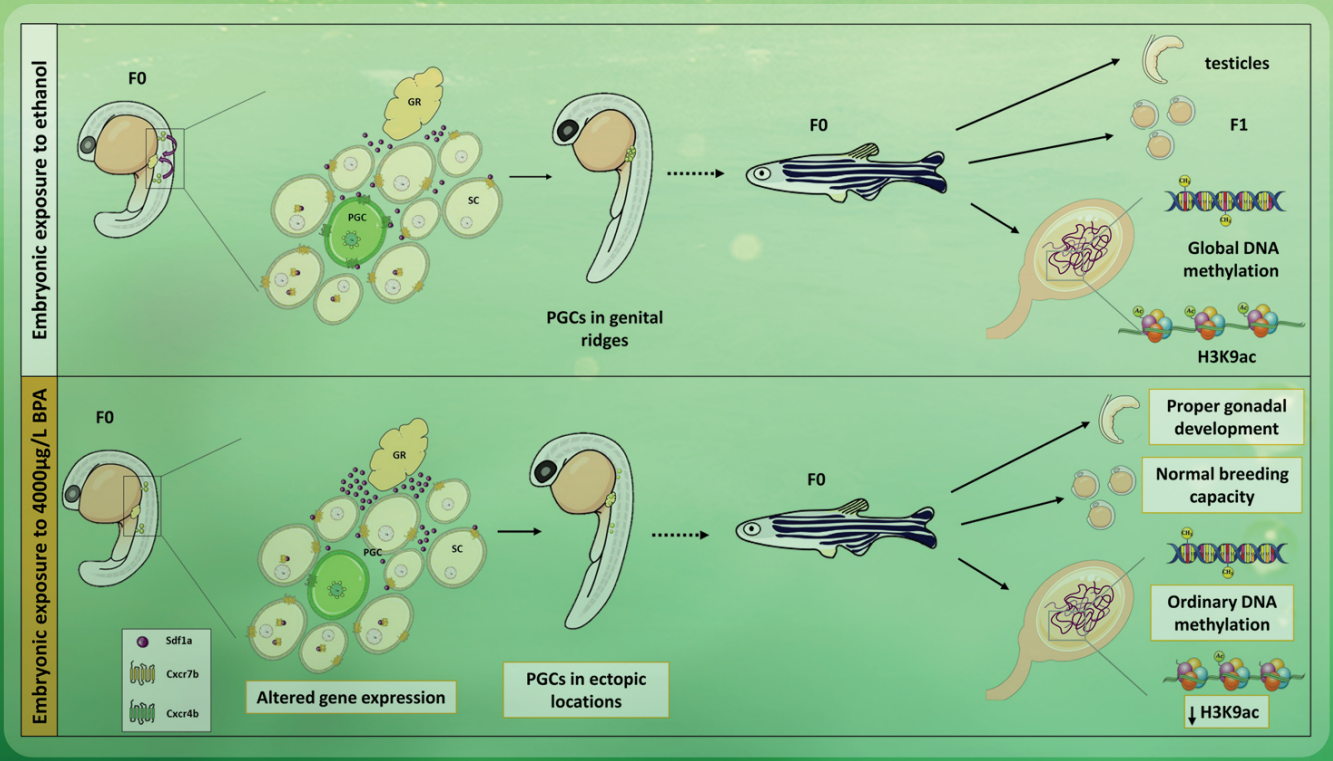

Embryonic Exposure to Bisphenol A Impairs Primordial Germ Cell Migration without Jeopardizing Male Breeding Capacity

Volume 9 · Issue 8 | August 2019

MDPI

mdpi.com/journal/biomolecules
ISSN 2218-273X

biomolecules

MDPI

Communication

Structural Changes in the Acceptor Site of Photosystem II upon Ca^{2+}/Sr^{2+} Exchange in the Mn_4CaO_5 Cluster Site and the Possible Long-Range Interactions

Faisal Hammad Mekky Koua [1,2,*]

[1] Center for Free Electron Laser Science, Deutsches Elektronen-Synchrotron (DESY), Notkestrasse 85, Hamburg 22607, Germany

[2] National University Biomedical Research Institute, National University-Sudan, Air St. P.O. Box 3783, Khartoum 11111, Sudan

Received: 19 July 2019; Accepted: 12 August 2019; Published: 14 August 2019

Abstract: The Mn_4CaO_5 cluster site in the oxygen-evolving complex (OEC) of photosystem II (PSII) undergoes structural perturbations, such as those induced by Ca^{2+}/Sr^{2+} exchanges or Ca/Mn removal. These changes have been known to induce long-range positive shifts (between +30 and +150 mV) in the redox potential of the primary quinone electron acceptor plastoquinone A (Q_A), which is located 40 Å from the OEC. To further investigate these effects, we reanalyzed the crystal structure of Sr-PSII resolved at 2.1 Å and compared it with the native Ca-PSII resolved at 1.9 Å. Here, we focus on the acceptor site and report the possible long-range interactions between the donor, $Mn_4Ca(Sr)O_5$ cluster, and acceptor sites.

Keywords: photosystem II; redox potential; electron transfer; charge separation; photoinhibition; water oxidation

1. Introduction

Photosystem II (PSII) is a large multisubunit membrane protein complex with at least 19 subunits. In physiological conditions, it exists as a dimer with a molecular weight of ca. 0.70 MDa and is embedded in the thylakoid membranes of oxygenic photosynthetic organisms [1]. PSII catalyzes one of the most fundamental reactions on Earth, that is, light-induced charge separation and water oxidation [1–3]. PSII initiates photosynthetic reactions by absorbing light through its internal antenna pigments. Light absorption leads to charge separation of the reaction center chlorophyll pigments, the so-called P680 molecules, and the process leads to the release of an electron and the formation of $P680^{\bullet+}$ and $Pheo^{\bullet-}$ ionic radicals [4–6]. Then, the released electron serves to reduce the plastoquinone molecule in the Q_A site, and the $Q_A/Q_A^{\bullet-}$ redox couple reduces a mobile Q_B with two consecutive electrons in the Q_B site, leading to the formation of plastoquinol (Q_BH_2) after taking up two protons from the stroma. Q_BH_2 then detaches from the Q_B site and moves into the plastoquinol pool in the membrane-spanning region [6]. The highly reactive $P680^{\bullet+}/Pheo^{\bullet-}$ and the subsequent secondary radical pairs formed by charge separation can be stabilized by oxidizing the catalytic center—the Mn_4CaO_5 cluster, which is also called the donor site—via a redox-active tyrosine (D1-Tyr161). P680 has the highest redox potential known in biology, E_m = 1.3 V (vs. standard hydrogen electrode [SHE]), which enables it to abstract electrons from and fully oxidize two water molecules by consecutively accumulating oxidizing equivalents in the Mn_4CaO_5 cluster during S*n*-state transitions, where n = 0–4 [5,6].

High-resolution XRD structures of PSII provide a detailed picture of the architecture of the protein matrix and the cofactor arrangements involved in the light-induced plastoquinone reduction and

water oxidation processes (Figure 1) [2,3]. However, the mechanistic basis of these processes, such as the role of Ca^{2+} in PSII light-induced water oxidation, is still not fully understood. Calcium has long been known as an essential element for water oxidation [3–7]. For example, Ca^{2+} removal was found to suppress the formation of higher oxidation states beyond the S_2 state [7]. This effect can be restored completely by Ca^{2+} or partially (ca. 40%–50%) by reconstituting Sr^{2+} in Ca^{2+}-depleted PSII [3,7–9]. This implies that there is a supervening rearrangement at the donor site of PSII and likely in other locations within the electron transfer (ET) chain. Indeed, fluorescence imaging of Sr-modified oxygen-evolving complex (OEC) PSII crystals showed altered properties of functional PSII, i.e., slowdown of the ET from Q_A to Q_B and stabilized $S_2Q_A^-$ charge recombination [10]. Consistent with this, modified ET kinetics at the donor site accompanied by conformational changes at the acceptor site were observed upon perturbations in the donor sites by Ca^{2+}/Sr^{2+} (but not by Cl^-/Br^-) exchanges, and this exchange upshifted the redox potential (E_m) of Q_A^-/Q_A by ~+30 mV [6,11]. Moreover, an even larger upshift in the E_m (Q_A/Q_A^-) of ~+150 mV and a relatively smaller shift (E_m = +20 mV) in non-heme iron (NHI) were previously reported for Mn-depleted PSII, and these shifts likely affect Ca^{2+} binding to the OEC [4]. These results indicate that the ET events between the donor and acceptor sites are highly tuned and governed not only by redox agents in the ET pathway but also by the protein moiety as well as the conformational changes near the OEC. The mechanism underlying the effects of these perturbations in the Mn_4CaO_5 cluster on the electrochemical properties of Q_A-Fe^{2+}-Q_B and the structural changes that take place in the acceptor site in response to such perturbations remain largely unclear. Note that the Mn_4CaO_5 cluster is far (~40 Å) from the acceptor site (Figure 1) [2,3].

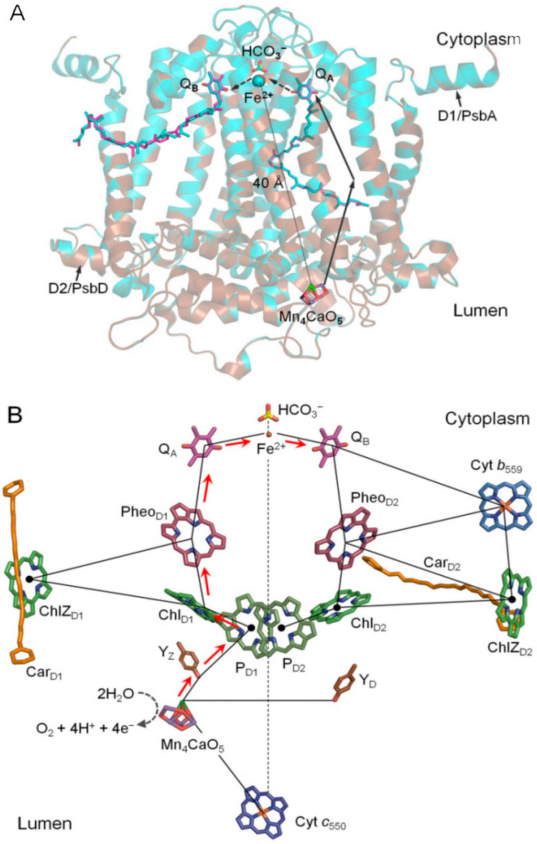

Figure 1. Electron transport pathway in the photosystem II complex. (**A**) Superimposed structures of the D1/D2 proteins from the native (cyan; PDB: 3WU2) and Sr-modified oxygen-evolving complex (OEC) (brown; PDB: 4IL6) photosystem II. The figure highlights the donor (Mn_4CaO_5 cluster) and the acceptor (Q_A-Fe^{2+}/HCO_3^--Q_B) sites, which are about 40 Å apart. (**B**) The electron transfer (ET) pathway and the locations of the main cofactors involved in the electron transfer process.

In our previous report on the Sr^{2+}-PSII structure resolved at 2.1 Å, we focused on the conformational changes that occur in the $Mn_4Ca(Sr)O_5$ cluster and its local environment [3]. To further investigate the possible effects of Ca^{2+}/Sr^{2+} exchange on the long-range interactions with the acceptor site, we revisited the structure of Sr-PSII (PDB: 4IL6) [3] and compared it with the native Ca-PSII model at a resolution of 1.9Å (PDB: 3WU2) [2]. The main focus was on the primary quinone electron acceptor (Q_A) site as well as the local environment of the acceptor site Q_A-Fe^{2+}-Q_B (Figure 1). It has been reported previously that OEC perturbations due to Ca^{2+}/Sr^{2+} exchange induce slight differences that are localized mainly in the OEC and nearby H-bonding networks mediated by water molecules. A significant change was observed at the W3 position: a Ca^{2+}/Sr^{2+}-bound water molecule, which might be responsible for the decrease in O_2 evolution by ~60% compared with the native PSII [2,3,12]. This is reasonable because the incorporation of Sr^{2+} takes place in the OEC site, and such conformational changes are expected to reduce the activity [3].

2. Materials and Methods

The crystal structure of Sr-PSII was resolved at 2.1 Å as described previously [3]. The structure factor files of Sr-PSII and the native Ca-PSII structure (PDB: 3WU2) were used to compare the structures and calculate the local root mean square deviation (rmsd) of the subunits PsbA/a and PsbD/d in the two structures using the DALI server. The PsbA/a and PsbD/d subunits provide the binding sites for Q_B and Q_A, respectively, as well as the NHI binding site. The overall rmsd between Sr-PSII (PDB: 4IL6) and Ca-PSII (3WU2) was calculated according to Cruickshank [13] using the SFCHECK program of the CCP4 suite [14], as mentioned in the original article [3]. In brief, the component precision index (DPI) was determined using the SFCHECK program, and the standard uncertainty value of the bond length between the two structures (rmsd) was obtained by multiplying the DPI value by the square root of 2. Further analyses and comparisons were performed using the Coot software, and the temperature factors in the selected regions of the proteins were estimated. All bond distances were obtained from the Coot program [15]. The least squares method was applied in Coot (LSQ Superpose) with the ranges of all atoms selected for the native Ca-PSII structure as a reference for comparison with the Sr-PSII mtz file. All figures were prepared using the software PyMOL (DeLano Scientific, San Carlos, CA, USA).

3. Results and Discussion

Figure 2 shows the structural comparison between Ca-PSII and Sr-PSII in the local vicinity of bicarbonate (BCT)-Fe^{2+}-His(4) and near the Q_A and Q_B sites. Q_A is located between the primary electron acceptor and the NHI site and mediates ET in PSII reactions (Figure 1) [2]. It is thus reasonable to attribute the shifts in the redox potential of Q_A to the structural changes that occur upon Mn/Ca depletion or Ca^{2+}/Sr^{2+} exchanges [5,10,11,16]. Q_A is stabilized by van der Waals interactions, including two moderate H-bonds between its carbonyl oxygen (C=O1, proximal; C=O2, distal) and N-Phe261-D2 and N_δ-His214-D2, respectively, as well as a π-stacking interaction with the nearby highly conserved D2-Trp253 (Table 1; Figure 3) [2,17]. This interaction is similar to the corresponding native Q_A interaction with slightly higher thermal motion, i.e., a 10%–20% increase in the temperature (B) factors (Table 1). This similarity indicated that the midpoint redox potential shifts (~+30 mV) that were observed upon Ca^{2+}/Sr^{2+} exchange were likely due to indirect effects or other H-bonding mediators or electrostatic forces. A recent study that applied attenuated total reflection (ATR)-FTIR difference spectroscopy excluded the direct influence of Mn_4CaO_5 cluster perturbations on the Q_A site [5]. D2-Thr217 was previously predicted to form an additional H-bond with the C=O (proximal) of Q_A and thus contribute to the positive shifts observed in the E_m (Q_A^-/Q_A) [12]. We observed that this residue formed a moderate H-bond with the indole nitrogen ($N_\varepsilon 1$) of the nearby D2-Trp253 (~2.8 Å), whereas it interacted weakly (through weak electrostatic interactions) with the proximal C=O of Q_A with a shorter H-bond (~–0.2 Å) in the Sr-PSII model. This finding implied the formation of a H-bond in Sr-PSII but not in Ca-PSII (~3.9 Å) (Figure 3A,B). These differences were similar between the two monomers of each model, although the differences lay roughly within the overall rmsd value (0.2 Å) of

the Cα atoms of Sr-PSII and Ca-PSII [2,3]. However, it is worth noting that the local rmsd values for the PsbD/A and Psba/d subunits between the two structures were 0.1 and 0.2 Å, respectively, as estimated by the DALI server. Such differences may give rise to different electrostatic energies between mediators and thus shift their redox potentials [18,19]. Notably, in the Ca^{2+}/Sr^{2+} exchange, the E_m (Q_A) shift was only ~+30 mV compared with +150 mV upon the depletion of Ca^{2+} or Mn(s) [4,5]. By comparing the H-bonding in the native structure with that in the Mn-depleted structure (PDB: 5MX2), we observed an even shorter bond distance (3.48 Å) between the proximal C=O with D2-Thr217, indicating the formation of an additional H-bond upon Mn depletion [20]. This agrees with the theoretical prediction and might be a cause of the upshifts in the E_m of Q_A [16]. Similar behavior was also observed in the H-bonding environment of the primary quinone acceptor of the bacterial reaction center (bRC) [21–23]. D2-Thr217 and D2-Trp253 are highly conserved between the bRC and PSII; thus, a similar mechanism is highly expected [2,24]. Interestingly, the structural changes upon Ca^{2+}/Sr^{2+} exchanges or Mn depletion gave rise to weaker H-bonds between the proximal C=O of Q_A and the imidazole nitrogen (N_δ) of D2-His214, with average distances of 2.79(+0.13) and 2.95(+0.29) Å, respectively [2,3,20]. The additional D2-Thr217 H-bond with Q_A resulted in a similar H-bonding environment between Q_A and Q_B (Figure 3A,B), which might be a cause of the decrease in the redox potential gap (ΔE_m) and hence a cause of the impairment of the forward ET combined with the enhancement of a direct charge recombination with P680 [25]. The perturbations of the His–Q_A interaction may affect their electrostatic coupling and perturb the E_m of Q_A. Moreover, the increased stabilization of Q_A due to an additional H-bond from D2-Thr217 could lead to the observed positive shift in the redox potential [16]. It should be noted that such positive shifts might vary, depending on the H-bond strength and hence the stability of Q_A. Therefore, the weak H-bond between D2-Thr217 and the C=O1 of Q_A in the Sr-PSII model might be the reason for the relatively smaller shifts, which were 70% lower than the E_m upshifts upon Ca/Mn removal [5,6].

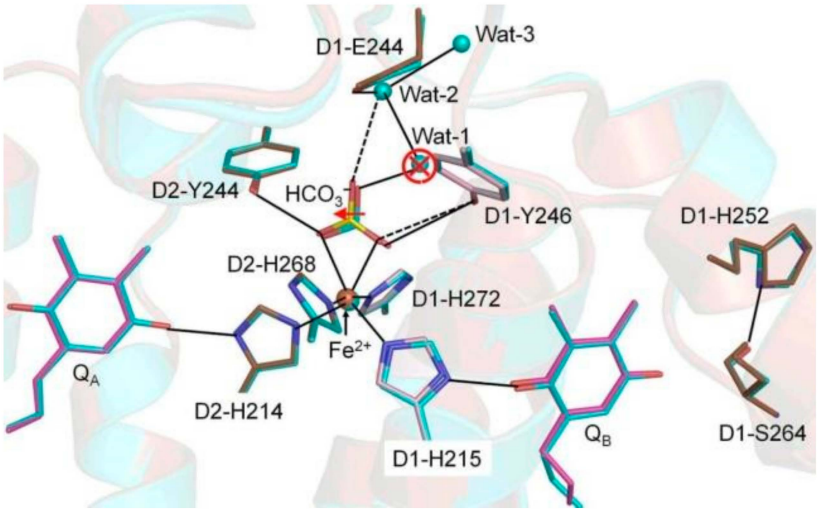

Figure 2. Superimposition of native Ca-PSII (PDB: 3WU2) and Sr-PSII (PDB: 4IL6) in the acceptor site pocket. The solid and dashed lines indicate that the hydrogen-bonding network within the acceptor site possibly facilitates the ET/proton transfer (PT) pathways that include two Q_A, Q_B, bicarbonate, non-heme iron (NHI), and water molecules. The red arrow and open circle indicate the major differences between native Ca-PSII and Sr-PSII.

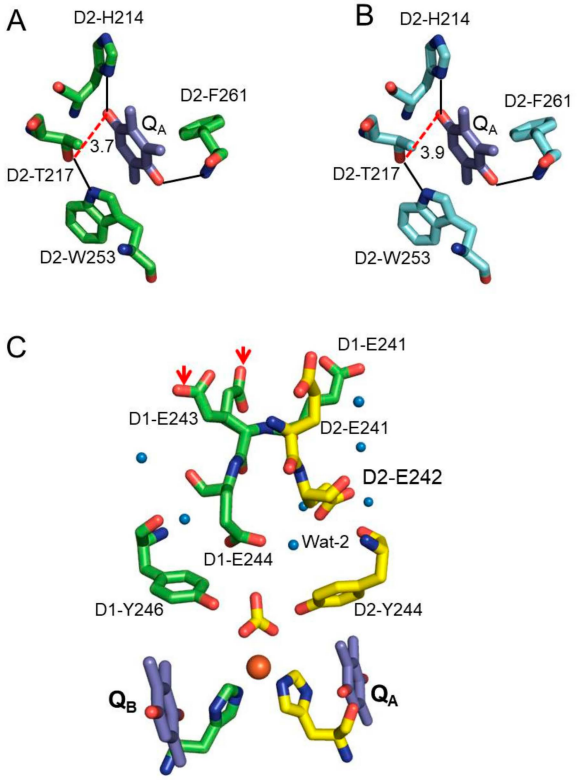

Figure 3. The immediate environment of Q_A and its relationships with the distant stromal Glu residues. (**A**) The interactions of Q_A with nearby residues and the additional H-bond (red dashed line) with D2-T217 and (**B**) the corresponding environment of Q_A in the Ca-PSII model. (**C**) The distant stromal Glu residues and associated water molecules. The red arrows indicate the rotamers of the D1-E243 residue in the Sr-PSII model.

We next analyzed the structural differences between Sr-PSII and Ca-PSII at the NHI site (Figure 2). NHI doesn't participate in the ET process between Q_A and Q_B. It binds four histidine residues, of which two residues—D2-His214 and D1-His215—form direct H-bonds with the proximal C=O of Q_A and Q_B, respectively [2]. Several differences between the two models were observed in the NHI site; for example, significant displacement was observed in the NHI of monomer A (0.42 Å). BCT, which binds NHI with a bidentate ligand via two C=O groups, was also significantly displaced in the Sr-PSII model by an average of 0.37 Å in the two monomers (Figure 2). This displacement led to significant changes in the H-bonding network within the immediate environment of NHI. In the Ca-PSII model, BCT forms H-bonds with the phenol hydroxyls of D1-Tyr246 and D2-Tyr244 with bond distances of 3.33 and 2.99 Å, respectively. These H-bond distances were significantly elongated in the Sr-PSII model, especially the H-bond with D1-Tyr246, which was elongated by +0.31 Å (3.64 Å). The role of BCT in PSII is controversial [26], but a recent report has claimed that it is involved in the redox tuning of PSII, perhaps by modulating its binding strength during the ET [27]. This might explain the perturbed interactions between BCT and NHI (Table 1) and D1-Tyr246 upon Ca^{2+}/Sr^{2+} exchange, and it is likely the reason for the positive shift in the E_m of Q_A.

Table 1. The average interatomic distances of the acceptor site of Sr-PSII (PDB: 4IL6) and native Ca-PSII (PDB: 3Wu2) and their corresponding temperature B-factors.

Ligand	Subunit	Sr-PSII (Å)	Ca-PSII (Å)	B-factor	Sr-PSII (Å^2)	Ca-PSII (Å^2)
Fe(II)						
				Fe(II)	29.61(0.42)	27.41(0.52)
NE2-His215	psbA/D1	2.06(0.02)	2.16(0.03)	NE2-His215	28.48(0.17)	25.75(0.79)
NE2-His214	psbD/D2	2.10(0.01)	2.17(0.07)	NE2-His214	27.24(1.97)	23.72(0.20)
NE2-His268	psbD/D2	2.20(0.02)	2.28(0.02)	NE2-His268	27.22(1.31)	24.37(0.30)
NE2-His272	psbA/D1	2.26(0.04)	2.26(0.01)	NE2-His272	29.67(0.94)	28.25(0.26)
O1-BCT	psbD/D2	2.30(0.02)	2.33(0.00)	O1-BCT	39.41(0.77)	31.23(0.24)
O2-BCT	psbD/D2	2.39(0.02)	2.29(0.05)	O2-BCT	39.74(0.68)	34.04(0.23)
Quinone B						
O1/ND1-His215	psbA/D1	2.50(0.00)	2.48(0.06)	O1/QB	52.37(0.55)	60.45(0.20)
O2/OG-Ser264	psbA/D1	2.76(0.06)	2.74(0.02)	O2/QB	52.73(0.53)	74.23(0.19)
O2/N-Phe265	psbA/D1	2.82(0.09)	2.95(0.05)	OG-Ser264	48.57(0.46)	63.62(0.17)
O2/O2-Phe265	psbA/D1	3.15(0.19)	3.09(0.08)	N-Phe265	47.07(0.51)	57.01(0.19)
				O2-Phe265	49.90(0.49)	66.33(0.18)
				ND1-His215	30.16(1.94)	27.23(0.16)
Quinone A						
O2/ND1-His214	psbD/D2	2.79(0.00)	2.66(0.06)	O2/QA	28.47(0.58)	25.13(0.21)
O1/N-Phe261	psbD/D2	3.02(0.00)	2.95(0.03)	O1/QA	28.60(0.62)	25.60(0.22)
				ND1-His214	27.32(0.47)	22.80(0.44)
				N-Phe261	26.74(0.45)	23.36(0.17)

Note: The values presented here are averages of two monomers, and the data in parentheses are the standard deviations between two monomers.

Recently, using FTIR difference spectroscopy, Kato et al. (2016) reported that the positive shifts in the mid-point redox potential of Q_A^-/Q_A might be due to modulation of the p*K*a of distant carboxylate residues in the stromal site of PSII [5]. There are indeed five Glu residues, namely, D1-Glu242, D1-Glu243, D1-Glu244, D2-Glu241, and D2-Glu242, ~15 Å from the NHI center and 55 Å from the Mn_4CaO_5 cluster toward the stromal side (Figure 3A,B) [2,3]. Together, these residues form extensive H-bonding networks involving several water molecules from the stromal site to the NHI center (Figure 3C). Two significant structural changes between Sr-PSII and Ca-PSII existed in this region. First, in the Sr-PSII model, the H-bonds between the C=O of BCT and the two water molecules, denoted wat-1 and wat-2, were broken as a result of the loss of wat-1 (Figure 2). Wat-1, in the Ca-PSII model, functions as a bridge between BCT and these Glu residues through an extensive H-bonding network, beginning with wat-2 and D1-Glu244 and proceeding to D1-Glu242 at the stromal site. In the Sr-PSII model, D1-Glu244 formed a weak H-bond with one C=O of BCT in the absence of wat-1 (Figure 2). Wat-1 also mediated the interaction between BCT and D1-Ser268 residue, which bind D1-His272, a ligand of NHI [2,3]. However, it was not clear whether the absence of this water molecule could cause such a shift in the redox potential of the Q_A site. Interestingly, wat-1 was preserved in the Mn-depleted structure of a single monomer, whereas both water molecules were absent from the second monomer [20]. The second difference was observed in one of the Sr-PSII monomers, in which the side chain of the D1-Glu243 residue formed two prominent rotamers with 0.5 occupancy for each monomer (Figure 3C). Such rotameric conformational changes may indicate the dynamic nature of D1-Glu243 and hence its involvement in the electrostatic interaction with the acceptor site. It is important to note that the similarity between the two monomers of PSII is still debated, so such differences between the two monomers cannot be excluded [28]. Further theoretical studies are required to clarify the effects of the modulation of the electrostatic interactions of these Glu residues on the redox potential of Q_A and their long-range interactions with the Mn_4CaO_5 cluster.

4. Conclusions

In summary, the present work highlights the structural changes that take place in the acceptor site of PSII upon perturbations of the Mn_4CaO_5 cluster due to Ca^{2+}/Sr^{2+} exchanges. We have shown that several structural changes occur at three different levels upon Ca^{2+}/Sr^{2+} exchanges: (i) the additional H-bonding at the Q_A site formed by D2-Thr217, (ii) the perturbations of BCT interactions with NHI and nearby Tyr residues, and (iii) the differences in the H-bonding network formed by distal Glu residues at the stromal side and the NHI binding site. Some of these structural changes might be responsible for the positive shifts in the mid-point redox potential of the primary quinone electron acceptor Q_A and hence impair the forward ET and enhance the backward ET and direct charge recombination between Q_A and $P680^+$, which is important for preventing the photoinhibition of PSII.

Funding: The author's research is funded by the European Research Council (ERC), grant no. 609920.

Acknowledgments: I would like to thank Shen Jian-Ren and Umena Yasufumi for their assistance in the Sr-PSII project at Okayama University. I would also like to acknowledge the financial support from the Japanese Governmental Scholarship (MEXT) program.

Conflicts of Interest: The author declares no conflict of interest.

References

1. Shen, J.-R. The structure of photosystem II and the mechanism of water oxidation in photosynthesis. *Ann. Rev. Plant. Biol.* **2015**, *66*, 23–48. [CrossRef]
2. Umena, Y.; Kawakami, K.; Shen, J.-R.; Kamiya, N. Crystal structure of oxygen-evolving photosystem II at a resolution of 1.9 Å. *Nature* **2011**, *473*, 55–60. [CrossRef]
3. Koua, F.H.M.; Umena, Y.; Kawakami, K.; Shen, J.-R. Structure of Sr-substituted photosystem II at 2.1 Å resolution and its implications in the mechanism of water oxidation. *Proc. Natl. Acad. Sci. USA* **2003**, *110*, 3889–3894. [CrossRef]
4. Kato, Y.; Noguchi, T. Long-Range Interaction between the Mn_4CaO_5 Cluster and the Non-heme Iron Center in Photosystem II as Revealed by FTIR Spectroelectrochemistry. *Biochemistry* **2014**, *53*, 4914–4923. [CrossRef]
5. Kato, Y.; Ishii, R.; Noguchi, T. Comparative analysis of the interaction of the primary quinone Q_A in intact and Mn-depleted photosystem II membranes using light-induced ATR-FTIR spectroscopy. *Biochemistry* **2016**, *55*, 6355–6358. [CrossRef]
6. Kato, Y.; Shibamoto, T.; Yamamoto, S.; Watanabi, T.; Ishida, N.; Sugiura, M.; Rappaport, F.; Boussac, A. Influence of the PsbA1/PsbA3, Ca^{2+}/Sr^{2+} and Cl^-/Br^- exchanges on the redox potential of the primary quinone Q_A in Photosystem II from *Thermosynechococcus elongatus* as revealed by spectroelectrochemistry. *Biochim. Biophys. Acta Bionenerg.* **2012**, *1817*, 1998–2004. [CrossRef]
7. Boussac, A.; Rappaport, F.; Carrier, P.; Verbavatz, J.M.; Gobin, R.; Kirilovsky, A.; Rutherford, A.W.; Sugiura, M. Biosynthetic Ca^{2+}/Sr^{2+} Exchange in the Photosystem II Oxygen-evolving Enzyme of *Thermosynechococcus elongatus*. *J. Biol. Chem.* **2004**, *279*, 22809–22819. [CrossRef]
8. Boussac, A.; Sugiura, M.; Rappaport, F. Probing the quinone binding site of photosystem II from *Thermosynechococcus elongatus* containing either PsbA1 or PsbA3 as the D1 protein through the binding characteristics of herbicides. *Biochim. Biophys. Acta Bioenerg.* **2011**, *1807*, 119–129. [CrossRef]
9. Krieger, A.; Rutherford, A.W.; Johnson, G.N. On the determination of redox midpoint potential of the primary quinone electron acceptor, Q_A, in photosystem II. *Biochim. Biophys. Acta Bioenerg.* **1995**, *1229*, 193–201. [CrossRef]
10. Kargul, J.; Maghlaoui, K.; Murray, J.W.; Deak, Z.; Boussac, A.; Rutherford, A.W.; Vass, I.; Barber, J. Purification, crystallization and X-ray diffraction analyses of the *T. elongatus* PSII core dimer with strontium replacing calcium in the oxygen-evolving complex. *Biochim. Biophys. Acta Bioenerg.* **2007**, *1767*, 404–413. [CrossRef]
11. Saito, K.; Rutherford, A.W.; Ishikita, H. Mechanism of proton-coupled quinone reduction in photosystem II. *Proc. Natl. Acad. Sci. USA* **2013**, *110*, 954–959. [CrossRef]
12. Chatterjee, R.; Milikisiyants, S.; Coates, C.S.; Koua, F.H.M.; Shen, J.R.; Lakshmi, K.V. The structure and activation of substrate water molecules in Sr^{2+}-substituted photosystem II. *Phys. Chem. Chem. Phys.* **2014**, *16*, 20834–20843. [CrossRef]

13. Cruickshank, D.W.J. Remarks about protein structure precision. *Acta Cryst. D* **1999**, *55*, 583–601. [CrossRef]
14. Collaborative Computational Project, Number 4. The CCP4 suite: Programs for protein crystallography. *Acta Cryst. D* **1994**, *50*, 760–763. [CrossRef]
15. Emsley, P.; Lohkamp, B.; Scott, W.G.; Cowtan, K. Features and development of Coot. *Acta Cryst. D* **2010**, *66*, 486–501. [CrossRef]
16. Ishikita, H.; Knapp, E.W. Control of quinone redox potentials in photosystem II: Electron transfer and photoprotection. *J. Am. Chem. Soc.* **2005**, *127*, 14714–14720. [CrossRef]
17. Chen, J.; Chen, J.; Liu, Y.; Zheng, Y.; Zhu, Q.; Han, G.; Shen, J.-R. Proton-coupled electron transfer of plastoquinone redox reactions in photosystem II: A pump-probe ultraviolet resonance Raman study. *J. Phys. Chem. Lett.* **2019**, *10*, 3240–3247. [CrossRef]
18. Moore, G.R.; Pettigrew, G.W.; Rogers, N.K. Factors influencing redox potentials of electron transfer proteins. *Proc. Natl. Acad. Sci. USA* **1986**, *83*, 4998–4999. [CrossRef]
19. Zhou, H.X.; Pang, X. Electrostatic interactions in protein structure, folding, binding, and condensation. *Chem. Rev.* **2018**, *118*, 1691–1741. [CrossRef]
20. Zhang, M.; Bommer, M.; Chatterjee, R.; Husseon, R.; Yano, J.; Dau, H.; Kern, J.; Dobbek, H.; Zouni, A. Structural insights into the light-driven auto-assembly process of the water-oxidizing Mn_4CaO_5-cluster in photosystem II. *Elife* **2017**, *6*, e2693.
21. Breton, J.; Boullais, C.; Burie, J.R.; Nabedryk, E.; Mioskowski, C. Binding sites of quinones in photosynthetic bacterial reaction centers investigated by light-induced FTIR difference spectroscopy: Symmetry of the carbonyl interactions and close equivalence of the Q_B vibrations in *Rhodobacter sphaeroides* and *Rhodopseudomonas viridis* probed by isotope labelling. *Biochemistry* **1994**, *33*, 14378–14386.
22. Brudler, R.; de Groot, H.J.M.; van Liemt, W.B.S.; Steggerda, W.F.; Esmeijer, R.; Gast, P.; Hoff, A.J.; Lugtenburg, J.; Gerwert, K. Asymmetric binding of the 1- and 4-C=O groups of Q_A in *Rhodobacter sphaeroides* R26 reaction centers monitored by Fourier transform infra-red spectroscopy using site-specific isotopically labelled ubiquinone-10. *EMBO J.* **1994**, *13*, 5523–5530. [CrossRef] [PubMed]
23. Zhu, Z.; Gunner, M.R. Energetics of quinone-dependent electron and proton transfers in Rhodobacter sphaeroides reaction centres. *Biochemistry* **2005**, *44*, 82–96. [CrossRef] [PubMed]
24. Ermler, U.; Fritzsch, G.; Buchanan, S.K.; Michel, H. Structure of the photosynthetic reaction center from *Rhodopbacter sphaeroides* at 2.65 Å resolution: Cofactors and protein-cofactor interactions. *Structure* **1994**, *2*, 935–936. [CrossRef]
25. Ashizawa, R.; Noguchi, T. Effects of hydrogen bonding interactions on the redox potential and molecular vibrations of plastoquinone as studied using density functional theory calculations. *Phys. Chem. Chem. Phys.* **2014**, *16*, 11864–11876. [CrossRef] [PubMed]
26. Shevela, D.; Eaton-Rye, J.J.; Shen, J.-R.; Govindjee. Photosystem II and the unique role of bicarbonate: A historical perspective. *Biochim. Biophs. Acta Bioenerg.* **2012**, *1817*, 1134–1151. [CrossRef]
27. Brinkert, K.; De Causmaecker, S.; Kriger-Liszkay, A.; Fantuzzi, A.; Rutherford, A.W. Bicarbonate-induced redox tuning in photosystem II for regulation and protection. *Proc. Natl. Acad. Sci. USA* **2016**, *113*, 1244–12149. [CrossRef] [PubMed]
28. Tanaka, A.; Fukushima, Y.; Kamiya, N. Two different structures of the oxygen-evolving complex in the same polypeptide frameworks of photosystem II. *J. Am. Chem. Soc.* **2017**, *139*, 1718–1721. [CrossRef]

© 2019 by the author. Licensee MDPI, Basel, Switzerland. This article is an open access article distributed under the terms and conditions of the Creative Commons Attribution (CC BY) license (http://creativecommons.org/licenses/by/4.0/).